

Multiple resonance and anti-resonance in coupled Duffing oscillators

R. Jothimurugan · K. Thamilmaran ·
S. Rajasekar · M. A. F. Sanjuán

Received: 9 February 2015 / Accepted: 8 October 2015
© Springer Science+Business Media Dordrecht 2015

Abstract We investigate the resonance behaviour in a system composed by n coupled Duffing oscillators where only the first oscillator is driven by a periodic force, assuming a nearest neighbour coupling. We have derived the frequency-response equations for a system composed of two coupled oscillators by using a theoretical approach. Interestingly, the frequency-response curve displays two resonance peaks and one anti-resonance. A theoretical prediction of the response amplitudes of two oscillators closely matches with the numerically computed amplitudes. We analyse the effect of the coupling strength on the resonance and anti-resonance frequencies and the response amplitudes at these frequencies. For the n coupled oscillators' system, in general, there are n -resonant peaks

and $(n - 1)$ anti-resonant peaks. For large values of n , except for the first resonance, other resonant peaks are weak due to linear damping. The resonance behaviours observed in the n coupled Duffing oscillators are also realized in an electronic analog circuit simulation of the equations. Understanding the role of coupling and system size has the potential applications in music, structural engineering, power systems, biological networks, electrical and electronic systems.

Keywords Coupled Duffing oscillators · Multiple resonance · Anti-resonance · Analog circuit simulation

1 Introduction

The typical frequency-response curve of a linear or nonlinear oscillator with a single degree of freedom subjected to an additive periodic driving force with a single frequency displays a single resonance peak. Furthermore, when the system is linear and undamped, the response amplitude becomes a maximum when the frequency of the driving force matches with the natural frequency of the system. In other oscillators, a single resonance peak occurs at a frequency different from their natural frequencies. For a system of n coupled linear oscillators where only the first oscillator is driven by an additive periodic force, for certain types of coupling, the frequency-response curve of each oscillator exhibits at most n peaks depending upon the values of the parameters of the oscillators [1]. The peaks are

R. Jothimurugan · K. Thamilmaran
Centre for Nonlinear Dynamics, School of Physics,
Bharathidasan University,
Tiruchirappalli, Tamilnadu 620 024, India
e-mail: jothi@cnd.bdu.ac.in

K. Thamilmaran
e-mail: maran.cnld@gmail.com

S. Rajasekar (✉)
School of Physics, Bharathidasan University,
Tiruchirappalli, Tamilnadu 620 024, India
e-mail: rajasekar@cnd.bdu.ac.in

M. A. F. Sanjuán
Nonlinear Dynamics, Chaos and Complex Systems Group,
Departamento de Física, Universidad Rey Juan Carlos,
Tulipán s/n, 28933 Móstoles, Madrid, Spain
e-mail: miguel.sanjuán@urjc.es

the resonances, and the corresponding frequencies are the resonant frequencies. The valleys in the frequency-response curve are the anti-resonant frequencies. There are $n - 1$ anti-resonant frequencies. In the absence of damping and for driving frequencies equal to the anti-resonant frequencies, the response amplitude vanishes. The multiple resonance and anti-resonance phenomena occur in nonlinear systems also as shown in the present work.

In the recent years, resonance is investigated on coupled systems also. For example, the coupling can enhance coherence resonance (CR) in Hodgkin–Huxley neuronal network [2]. The onset and control of stochastic resonance in two mutually coupled driven bistable systems subjected to independent noises are investigated [3]. In a coupled bistable system, coupling improves the reliability of the logic system and thus enhances the logical stochastic resonance effect. Moreover, enhancement is larger for larger system size, whereas for large enough size the enhancement seems to be saturated [4]. System size resonance and coherence resonance are demonstrated using coupled noisy systems, Ising model [5] and FitzHugh–Nagumo model [6]. Effect of vibrational resonance of neuronal systems depends extensively on the network structure and parameters, such as the coupling strength between neurons, network size, and rewiring probability of single small-world networks, as well as the number of links between different subnetworks and the number of subnetworks in the modular networks [7]. The enhanced signal propagation is achieved in the coupled Duffing oscillators in the realm of ghost vibrational resonance [8]. Mechanisms of fano resonances are demonstrated by both theoretically and experimentally in coupled plasmonic system [9]. Very recently, the influence of nonlinearities on the collective dynamics of coupled Duffing–van der Pol oscillators subjected to both parametric and external perturbations has been reported [10].

Why is the study of anti-resonance important? What are its real practical applications? Details of anti-resonance are useful in the design of chemotherapeutic protocols [11], dynamic model updating [12–15] and desynchronizing undesired oscillations [16]. Driving a piezoelectronic motor at anti-resonant frequencies has also practical advantages [17]. Anti-resonance is employed to minimize unwanted vibrations of certain parts of a system in mechanical engineering and aerospace industries. In the vibration control of fixture, controlling anti-resonant frequencies is more impor-

tant than resonant frequencies since the worst case can occur at anti-resonance [18, 19]. In a vibratory structural system, an addition of mass is found to shift the resonant frequencies without affecting the anti-resonant frequencies [20]. It has been pointed out that a shift of the resonant frequencies beyond anti-resonance is not feasible. Anti-resonance has been realized also in quantum systems [21, 22].

In the recent past, several studies are reported to uncover the underlying theory of anti-resonance. Particularly, stochastic anti-resonance is investigated in a theoretical model equation proposed for the transmission of a periodic signal mixed with a noise through static nonlinearity [23], squid axon model equation [24], the time evolution of interacting qubits of quantum systems [25] and certain piecewise linear systems [26]. Coherence anti-resonance is identified in a model of circadian rhythmicity in *Drosophila* [27] and in FitzHugh–Nagumo neuron model [28] subjected to both additive and multiplicative noise. The anti-resonance is demonstrated in a parametrically driven van der Pol oscillator and illustrated a two-state switch by using two coupled oscillators [29]. A single or two coupled systems are investigated in these studies with theoretical and numerical treatment. It is vital to study n coupled, nonlinear systems in the vicinity of multiple and anti-resonances.

Further, it is of great significance to investigate the response of coupled systems with the first unit alone subjected to external periodic force. Such a set-up finds applications in digital sonar arrays, network of sensory neurons, vibrational resonance, stochastic resonance and signal propagation in coupled systems [30–34]. We report our investigation on the resonant and anti-resonant dynamics in a system of two coupled and n coupled Duffing oscillators. The occurrence of multiple and anti-resonance is presented using theoretical, numerical and experimental methods. The connection between the coupling strength and occurrence of multiple and anti-resonance, and the role of system size on the n coupled systems are the important significances of the present work. In this system, the oscillators are allowed to interact with their nearest neighbour with a linear coupling. Furthermore, we consider that only the first oscillator is subjected to a periodic driving force. For a system of two coupled oscillators and using a theoretical approach, we obtain coupled equations for the response amplitudes $Q_1 = A_1/f$ and $Q_2 = A_2/f$ where A_1 and A_2 are the amplitudes of the periodic

oscillations of the oscillator-1 and oscillator-2, respectively, and f is the amplitude of the external periodic driving force. The theoretically predicted values of Q_1 and Q_2 are found to match very closely with the values of Q_1 and Q_2 computed numerically. When the frequency of the driving force is varied, two resonant peaks and one anti-resonance occur for a wide range of fixed values of the coupling strength δ . We analyse the dependence of the resonant and anti-resonant frequencies and the values of the response amplitudes of these two oscillators on the coupling parameter δ . For the n coupled systems, since theoretical analysis is very difficult and involves solving of n coupled nonlinear equations for the amplitudes A_i s, we analyse the occurrence of resonant and anti-resonant behaviours by numerically solving the system of equations of motion. The n coupled oscillators are found to show n resonances and $n - 1$ anti-resonances. We study the dependence of the resonant and anti-resonant frequencies with the number n of oscillators that are coupled. The resonance and the anti-resonance behaviours found in theoretical model equations are also realized in an analog electronic circuit simulation of the equations. Hardware experimental analog simulation studies on two coupled and PSpice simulation of n coupled oscillators shows good agreement with the theoretical/numerical predictions.

2 Periodically driven two coupled systems

The equation of motion of the n coupled Duffing oscillators of our interest is

$$\ddot{x}_1 + d\dot{x}_1 + \omega_0^2 x_1 + \beta x_1^3 + \delta(x_1 - x_2) = f \cos \omega t, \tag{1a}$$

$$\ddot{x}_i + d\dot{x}_i + \omega_0^2 x_i + \beta x_i^3 + \delta(x_i - x_{i-1}) + \delta(x_i - x_{i+1}) = 0, \tag{1b}$$

$$\ddot{x}_n + d\dot{x}_n + \omega_0^2 x_n + \beta x_n^3 + \delta(x_n - x_{n-1}) = 0. \tag{1c}$$

In this system, the first and the last oscillators are not connected to each other and δ is the strength of the coupling. We start with the simplest case $n = 2$ that is a system of two coupled oscillators.

2.1 Theoretical treatment

By applying a perturbation approach, a frequency-response equation can be obtained. We assume a periodic solution of the system (1) with $n = 2$ as

$$x_i(t) = a_i(t) \cos \omega t + b_i(t) \sin \omega t \tag{2}$$

with a_i and b_i to be determined, which are slowly varying functions of time. We substitute

$$\dot{x}_i(t) = \dot{a}_i \cos \omega t + \dot{b}_i \sin \omega t - a_i \omega \sin \omega t + b_i \omega \cos \omega t, \tag{3a}$$

$$\ddot{x}_i(t) = -2\dot{a}_i \omega \sin \omega t + 2\dot{b}_i \omega \cos \omega t - a_i \omega^2 \cos \omega t - b_i \omega^2 \sin \omega t, \tag{3b}$$

$$x_i^3 \approx \frac{3}{4} (a_i^2 + b_i^2) (a_i \cos \omega t + b_i \sin \omega t), \tag{3c}$$

where in Eq. (3b) \ddot{a}_i and \ddot{b}_i are neglected due to their smallness, in Eqs. (1), and then neglect $d\dot{a}_i$ and $d\dot{b}_i$ because they are assumed to be small. Next, equating the coefficients of $\sin \omega t$ and $\cos \omega t$ separately to zero gives

$$\dot{a}_1 = \frac{b_1}{2\omega} \left[\omega_0^2 - \omega^2 + \delta + \frac{3\beta}{4} (a_1^2 + b_1^2) \right] - \frac{da_1}{2} - \frac{\delta b_2}{2\omega}, \tag{4a}$$

$$\dot{b}_1 = -\frac{a_1}{2\omega} \left[\omega_0^2 - \omega^2 + \delta + \frac{3\beta}{4} (a_1^2 + b_1^2) \right] - \frac{db_1}{2} + \frac{\delta a_2}{2\omega} + \frac{f}{2\omega}, \tag{4b}$$

$$\dot{a}_2 = \frac{b_2}{2\omega} \left[\omega_0^2 - \omega^2 + \delta + \frac{3\beta}{4} (a_2^2 + b_2^2) \right] - \frac{da_2}{2} - \frac{\delta b_1}{2\omega}, \tag{4c}$$

$$\dot{b}_2 = -\frac{a_2}{2\omega} \left[\omega_0^2 - \omega^2 + \delta + \frac{3\beta}{4} (a_2^2 + b_2^2) \right] - \frac{db_2}{2} + \frac{\delta a_1}{2\omega}. \tag{4d}$$

Equations (4) under the transformation

$$a_i(t) = A_i(t) \cos \theta_i(t), \quad b_i(t) = A_i(t) \sin \theta_i(t) \tag{5}$$

take the form (with $A_i^2 = a_i^2 + b_i^2$)

$$\dot{A}_1 = -\frac{dA_1}{2} + \frac{\delta A_2}{2\omega} \sin(\theta_1 - \theta_2) + \frac{f}{2\omega} \sin \theta_1 = P, \tag{6a}$$

$$A_1 \dot{\theta}_1 = -\frac{A_1}{2\omega} \left[\omega_0^2 - \omega^2 + \delta + \frac{3\beta}{4} A_1^2 \right] + \frac{\delta A_2}{2\omega} \cos(\theta_1 - \theta_2) + \frac{f}{2\omega} \cos \theta_1 = Q, \tag{6b}$$

$$\dot{A}_2 = -\frac{dA_2}{2} - \frac{\delta A_1}{2\omega} \sin(\theta_1 - \theta_2) = R, \tag{6c}$$

$$A_2 \dot{\theta}_2 = -\frac{A_2}{2\omega} \left[\omega_0^2 - \omega^2 + \delta + \frac{3\beta}{4} A_2^2 \right] + \frac{\delta A_1}{2\omega} \cos(\theta_1 - \theta_2) = S. \tag{6d}$$

For a periodic solution, in the long time limit, $A_i(t) \rightarrow A_i^*$ and $\theta_i(t) \rightarrow \theta_i^*$. (A_i^*, θ_i^*) is an equilibrium point of Eqs. (6). We set $\dot{A}_i = 0, \dot{\theta}_i = 0$, drop ‘*’ in A_i^* and θ_i^* and then eliminate θ_i ’s. We obtain the set of equations

$$A_1^2 \left[u_1^2 + d^2 \omega^2 \right] + \left[2d^2 \omega^2 + \delta^2 \right] A_2^2 - 2u_1 u_2 A_2^2 = f^2, \tag{7a}$$

$$A_2^2 \left[u_2^2 + d^2 \omega^2 \right] - \delta^2 A_1^2 = 0, \tag{7b}$$

$$\theta_1 = \tan^{-1} \left[\frac{d\omega(A_1^2 + A_2^2)}{A_1^2 u_1 - A_2^2 u_2} \right], \tag{7c}$$

$$\theta_2 = \theta_1 - \tan^{-1} \left[-\frac{d\omega}{u_2} \right], \tag{7d}$$

where

$$u_i = \omega_0^2 - \omega^2 + \delta + \frac{3\beta}{4} A_i^2, \quad i = 1, 2. \tag{7e}$$

The stability of the equilibrium point $(A_1^*, A_2^*, \theta_1^*, \theta_2^*)$ of Eqs. (6) can be determined by linear stability analysis. The stability determining eigenvalues can be obtained from

$$\begin{vmatrix} \frac{\partial P}{\partial A_1} - \lambda & \frac{\partial P}{\partial \theta_1} & \frac{\partial P}{\partial A_2} & \frac{\partial P}{\partial \theta_2} \\ \frac{\partial Q}{\partial A_1} & \frac{\partial Q}{\partial \theta_1} - \lambda & \frac{\partial Q}{\partial A_2} & \frac{\partial Q}{\partial \theta_2} \\ \frac{\partial R}{\partial A_1} & \frac{\partial R}{\partial \theta_1} & \frac{\partial R}{\partial A_2} - \lambda & \frac{\partial R}{\partial \theta_2} \\ \frac{\partial S}{\partial A_1} & \frac{\partial S}{\partial \theta_1} & \frac{\partial S}{\partial A_2} & \frac{\partial S}{\partial \theta_2} - \lambda \end{vmatrix} = 0, \tag{8}$$

where the partial derivatives are evaluated at the equilibrium point. Expanding the determinant, we obtain the characteristic equation of the form

$$a_4 \lambda^4 + a_3 \lambda^3 + a_2 \lambda^2 + a_1 \lambda + a_0 = 0. \tag{9}$$

The equilibrium point $(A_1^*, A_2^*, \theta_1^*, \theta_2^*)$ is stable if all the eigenvalues of Eq. (9) has negative real part; otherwise, it is unstable. For a stable $(A_1^*, A_2^*, \theta_1^*, \theta_2^*)$, the system-(1) exhibits a stable periodic solution.

2.2 Two coupled linear systems

We consider now the case of two coupled linear and undamped oscillators [$n = 2, \beta = 0$ and $d = 0$ in Eqs. (1)] [1] whose amplitudes A_1 and A_2 which are obtained from Eqs. (7) are

$$A_1 = \frac{f(\omega_0^2 - \omega^2 + \delta)}{(\omega_0^2 - \omega^2)(\omega_0^2 - \omega^2 + 2\delta)}, \tag{10a}$$

$$A_2 = \frac{\delta A_1}{(\omega_0^2 - \omega^2 + \delta)} = \frac{\delta f}{(\omega_0^2 - \omega^2)(\omega_0^2 - \omega^2 + 2\delta)}. \tag{10b}$$

Both A_1 and A_2 are a maximum at $\omega = \omega_0$ and $\sqrt{\omega_0^2 + 2\delta}$. The amplitude A_1 becomes minimum when the term $(\omega_0^2 - \omega^2 + \delta)$ in Eq. (10a) is a minimum.

This happens at $\omega = \sqrt{\omega_0^2 + \delta}$. Thus, the frequency at which anti-resonance occurs in oscillator-1 is $\omega_{1,ar} = \sqrt{\omega_0^2 + \delta}$. At $\omega_{1,ar}, A_{1,ar} = 0$. From Eq. (10b), it is reasonable to expect A_2 to be a minimum at a frequency ω at which A_1 becomes a minimum. Substitution of $\omega^2 = \omega_{1,ar}^2 = \omega_0^2 + \delta$ in Eq. (10b) gives $A_{2,ar} = f/\delta \neq A_{1,ar}$ and is nonzero.

For the damped ($d \neq 0$) and linear system, we have

$$A_1 = \left(\frac{f^2 u_+}{u_+^2 + \delta^4 - 2\delta^2 u_-} \right)^{1/2}, \tag{11a}$$

$$A_2 = \frac{\delta A_1}{\sqrt{u_+}}, \quad u_{\pm} = (\omega_0^2 - \omega^2 + \delta)^2 \pm d^2 \omega^2. \tag{11b}$$

It is difficult to obtain explicit expressions for the two resonant frequencies and the corresponding amplitudes due to the complexity of the expressions of A_1 and A_2 . However, the anti-resonant frequency can be determined by seeking the value of ω at which the quantity u_+ becomes a minimum. This gives

$$\omega_{1,ar} = \sqrt{\omega_0^2 + \delta - \frac{d^2}{2}}. \tag{12}$$

2.3 Two coupled Duffing oscillators

Now, we consider the two coupled Duffing oscillators. Decoupling of the amplitudes in Eqs. (7) is very difficult. However, applying the Newton–Raphson method [35] developed for coupled equations, various possible

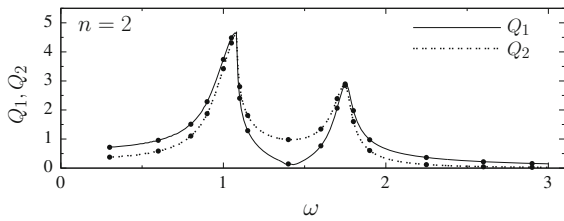


Fig. 1 Response amplitudes Q_1 (of oscillator-1) and Q_2 (of oscillator-2) versus the frequency ω of the driving force of the two coupled Duffing oscillators, Eqs. (1) with $n = 2$. The *continuous* and *dotted curves* are the theoretically predicted Q_1 and Q_2 , respectively. The *solid circles* are the numerical ones. Here $d = 0.1$, $\omega_0^2 = 1$, $\beta = 1$, $\delta = 1$ and $f = 0.1$

values of A_1 and A_2 can be determined, and then, the frequency-response curve can be drawn.

We choose the values of the parameters as $d = 0.1$, $\omega_0^2 = 1$, $\beta = 1$ and $\delta = 1$. Figure 1 presents both theoretical $Q_i (=A_i/f)$ and numerically computed Q_i , $i = 1, 2$ as a function of the driving frequency ω . The theoretical prediction matches very closely the numerical results obtained from the simulations. Q_1 is a maximum at $\omega = 1.08$ and also at $\omega = 1.75$. Q_2 becomes a maximum at $\omega = 1.08$ and at 1.74 . Anti-resonance in Q_1 and Q_2 occurs at $\omega_{1,ar} = 1.43$ and $\omega_{2,ar} = 1.42$. However, $Q_{1,ar} = 0.1181$, while $Q_{2,ar} = 0.9804$. In order to show the significant effects of the linear coupling constant δ on the resonant dynamics, we display the dependence of Q_1 and Q_2 versus ω on the parameter δ in Fig. 2. Q_1 has a single resonance for $0 < \delta < 0.1$ and two resonant peaks for $\delta \geq 0.1$. For the second oscillator, a double resonance is realized for $\delta \geq 0.13$.

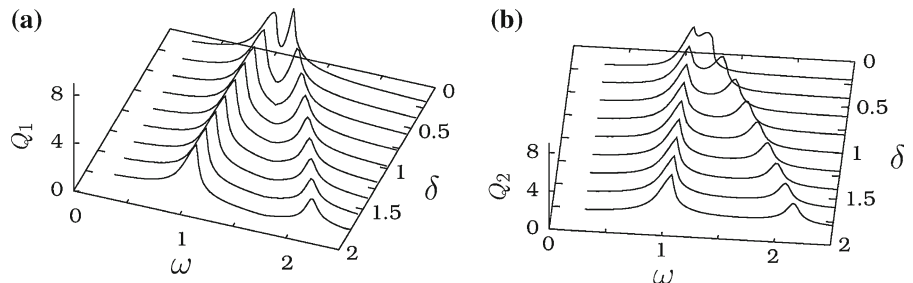
We denote $\omega_{i,r}^{(j)}$ as the value of ω at which the i th resonance occurs in the j th oscillator. And $Q_{i,r}^{(j)}$ is the value of the response amplitude at $\omega_{i,r}^{(j)}$. For $n = 2$, there is only one anti-resonance. Therefore, we denote $\omega_{1,ar}$ and $\omega_{2,ar}$ as the values of ω at which anti-resonance occurs in the oscillators 1 and 2, respectively, and the corresponding values of Q as $Q_{1,ar}$ and

$Q_{2,ar}$, respectively. These quantities are computed for a range of values of δ . Figure 3a displays the variation in $\omega_{1,r}^{(1)}$ (continuous curve), $\omega_{2,r}^{(1)}$ (dotted curve), $\omega_{1,r}^{(2)}$ (solid circles) and $\omega_{2,r}^{(2)}$ (open circles) with δ . The first resonant frequencies of both oscillators are almost the same and independent of δ , except for $\delta \ll 1$. In contrast to this, the second resonant frequencies of the two oscillators vary with δ ; however, $\omega_{2,r}^{(1)} \approx \omega_{2,r}^{(2)}$ for each fixed value of δ , except for $\delta \ll 1$. In Fig. 3b $Q_{1,r}^{(j)}$, $j = 1, 2$ approach the same constant value where as $Q_{2,r}^{(j)}$, $j = 1, 2$ decrease for increasing values of δ .

The dependence of anti-resonance frequencies and the corresponding amplitudes of the oscillations on the coupling strength δ are plotted in Fig. 4. In this figure, the numerical results are represented by symbols and the appropriate curve fits are marked by continuous curves. Furthermore, the frequencies $\omega_{1,ar}$ and $\omega_{2,ar}$ are found to depend linearly on δ . We obtain $\omega_{1,ar} = 1.0759 + 0.325\delta$ and $\omega_{2,ar} = 1.079 + 0.325\delta$. In the linear system ($\beta = 0$), as noted earlier, $\omega_{1,ar} = \sqrt{\omega_0^2 + \delta} \approx 1 + 0.5\delta$. $Q_{1,ar}$ and $Q_{2,ar}$ decrease rapidly following the power-law relations $0.14106\delta^{-1.696}$ (for $\delta > 0.1$) and $0.939\delta^{-0.881}$ (for $\delta > 0.13$), respectively. That is, by increasing the value of δ , the anti-resonant frequency is increased, while the response amplitude at the anti-resonance is reduced. In Fig. 4, $\omega_{1,ar}^{(1)} \approx \omega_{2,ar}^{(2)}$, but $Q_{1,ar} < Q_{2,ar}$ for a wide range of values of δ . By increasing the value of the damping coefficient, the response amplitudes decrease, and for sufficiently large values, the second resonance in both oscillators is suppressed.

One of the features of the resonance in nonlinear oscillators is the appearance of hysteresis in the frequency-response curve. This is also realized in the system (1) near two resonances for certain range of values of β . An example is presented in Fig. 5 for $\beta = 20$ and $\delta = 1$. In both oscillators, two stable

Fig. 2 Response amplitudes **a** Q_1 and **b** Q_2 as a function of the parameters δ and ω for the system (1) with $n = 2$, $d = 0.1$, $\omega_0^2 = 1$, $\delta = 1$ and $f = 0.1$



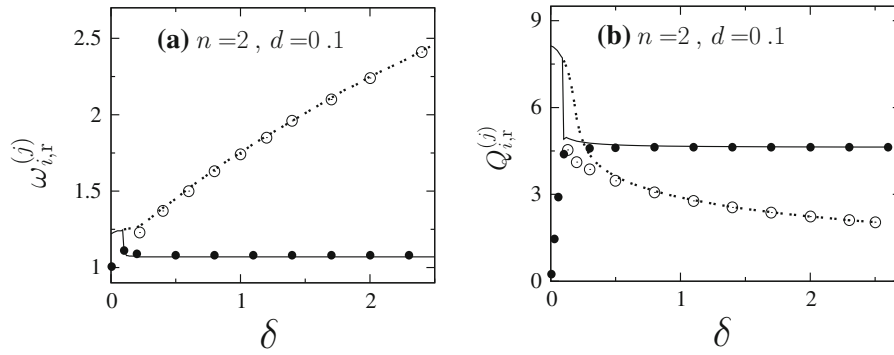


Fig. 3 Dependence of **a** resonant frequencies and **b** the response amplitudes at the resonant frequencies as a function of the coupling constant δ of the two coupled Duffing oscillators. In both subplots, the *continuous* and *dotted lines* are associated with the

first and second resonances of the first oscillator, respectively. The *solid* and *open circles* correspond to the first and second resonances of the second oscillator, respectively. Here $d = 0.1$, $\omega_0^2 = 1$, $\beta = 1$ and $f = 0.1$

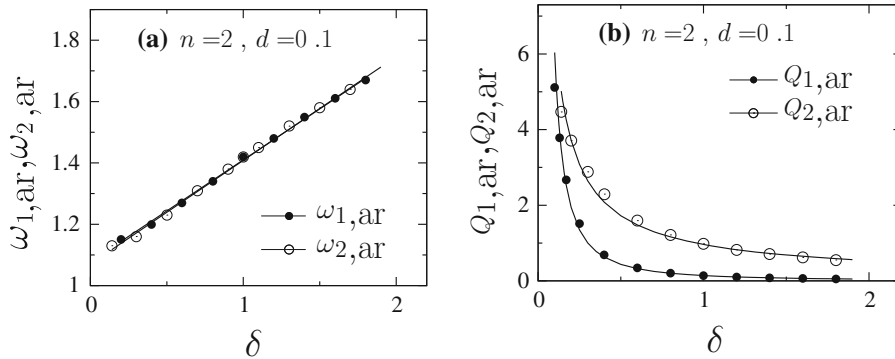


Fig. 4 Variation in **a** anti-resonant frequencies $\omega_{1,ar}$ and $\omega_{2,ar}$ of the first and second oscillators, respectively, and **b** response amplitude of the anti-resonance with the coupling strength δ of

the two coupled Duffing oscillators, Eqs. (1) with $n = 2$. The *symbols* are numerical data, and *continuous curves* are the best fit

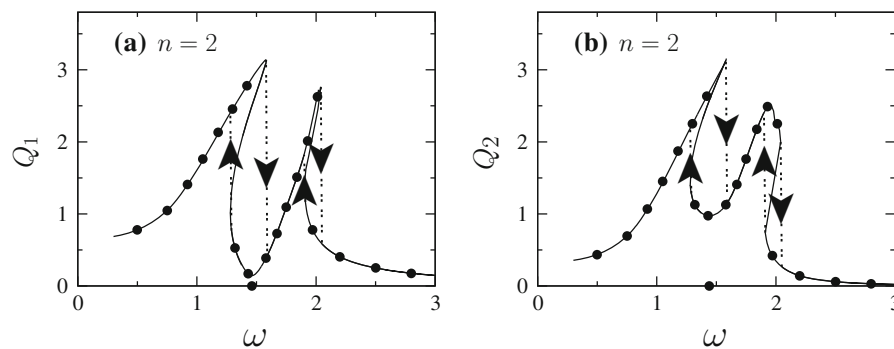


Fig. 5 Frequency-response curves of **a** oscillator-1 and **b** oscillator-2 of the two coupled Duffing oscillators [Eqs. (1)] with $n = 2$. The *continuous curve* and the *solid circles* are the theoretically predicted and numerically computed values of response amplitudes. The *solid circle* on the ω axis marks the value of ω

at which anti-resonance occurs. In both subplots, the *downward* and *upward arrows* indicate the jump in the response amplitudes when the frequency is varied in the forward and backward directions, respectively. The values of the parameters are $d = 0.1$, $\omega_0^2 = 1$, $\beta = 20$, $\delta = 1$ and $f = 0.1$

periodic orbits with different amplitudes coexist for $\omega \in [1.28, 1.58]$ and $[1.9, 2.04]$. In these intervals, the theoretical response curve has three branches. The upper branch and lower branch are realized when the frequency is swept in the forward and backward directions, respectively. These are stable branches and are observed in the numerical simulations, as well. For each ω in the intervals $[1.28, 1.58]$ and $[1.9, 2.04]$, there exist two periodic orbits with different amplitudes. They are observed for different set of initial conditions. The middle branch is not realized in the numeri-

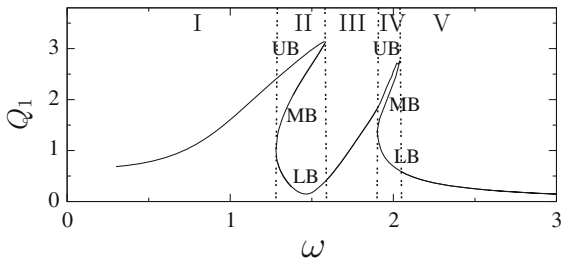


Fig. 6 Frequency-response curve of oscillator-1. The intervals I, II and V have only one stable periodic orbit, and the remaining intervals have three branches in which the upper branch (UB) and lower branch (LB) correspond to stable periodic orbits, while the middle branch (MB) correspond to a unstable periodic orbit. The values of the parameters are $d = 0.1, \omega_0^2 = 1, \beta = 20, \delta = 1$ and $f = 0.1$

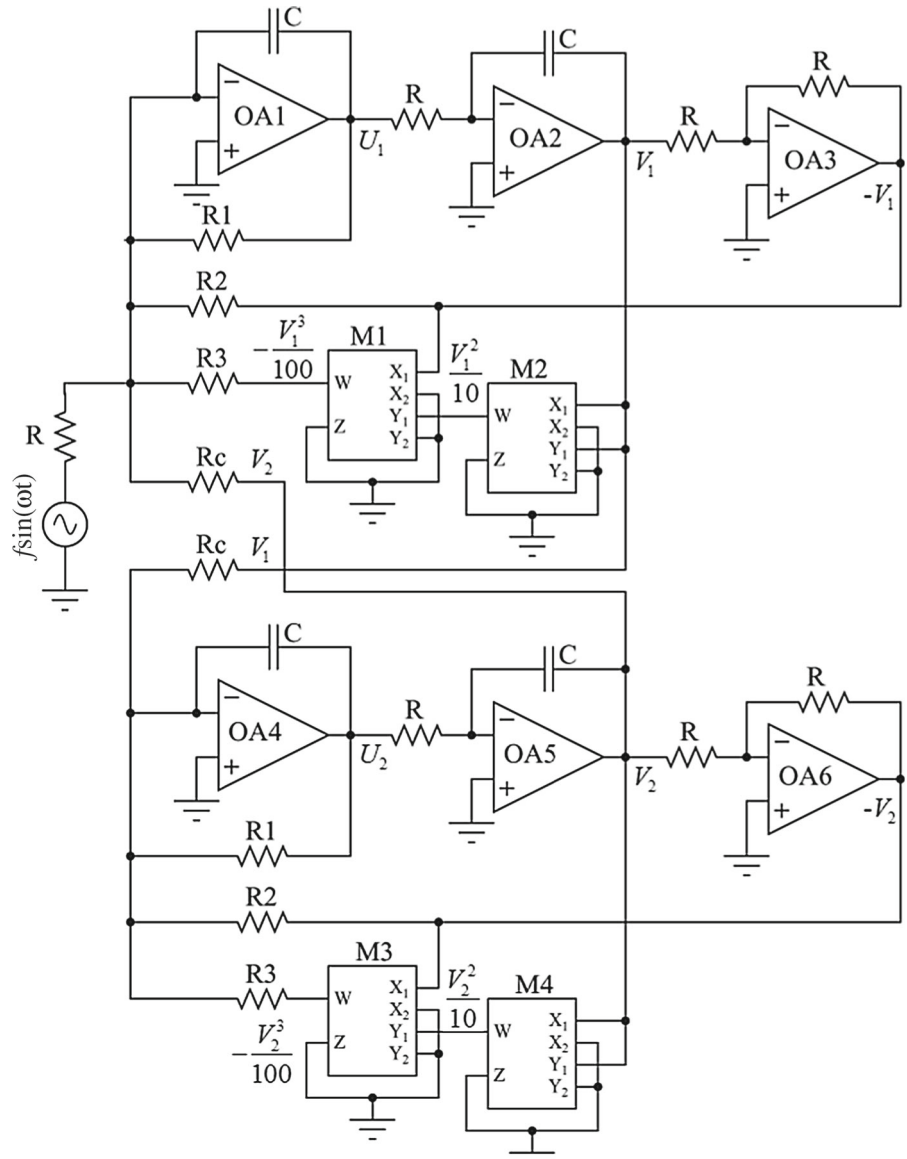
cal simulations for a large set of initial conditions and is an unstable branch. When ω is increased from a small value, a first resonance in both oscillators occurs at $\omega = 1.58$ but with $Q_1 = 3.14$ and $Q_2 = 3.11$. The second resonance in the oscillators 1 and 2 takes place at $\omega = 2.04$ and 1.95 , respectively, with $Q_1 = 2.76$ and $Q_2 = 2.52$.

The stability analysis of equilibrium points of Eqs. 6 is performed to determine the stability of the periodic orbits of the system (1). From Eqs. (7a) and (7b), A_i s are calculated which are then substituted in Eqs. (7c) and (7d) to get θ_i s. These $(A_1^*, A_2^*, \theta_1^*, \theta_2^*)$ s calculated for various values of ω are applied to Eq. (9) to obtain the eigenvalues of the characteristic equation. The frequency response curve is classified into five segments as shown in Fig. 6. The odd-numbered segments have only one $(A_1^*, A_2^*, \theta_1^*, \theta_2^*)$. Complex conjugate eigenvalues with negative real part are obtained in these regions. This implies that $(A_1^*, A_2^*, \theta_1^*, \theta_2^*)$ is stable in these region. Hence, the periodic orbit in these regions is stable. In the even-numbered intervals of ω , there are three equilibrium points and are classified into three branches. The upper and lower branches (UB and LB) have the complex conjugate eigenvalues with negative real part, while the middle branch (MB) has an eigenvalue with positive real part. Hence, the UB and LB are stable, while the MB is unstable. Table 1 presents

Table 1 The equilibrium points and their stability determining eigenvalues for certain values of ω corresponding to Fig. 6

Region in ω	ω	A_1^*	A_2^*	θ_1^*	θ_2^*	Eigenvalues	Nature of stability
I	1.0	0.16076	0.12828	0.26899	0.34902	$-0.05024 \pm i1.31391,$ $-0.05019 \pm i0.27370$	Stable
II	1.35	0.25929	0.24097	0.73131	0.85937	$-0.05060 \pm i1.08736,$ $-0.05057 \pm i0.19524$	Stable
	1.35	0.18618	0.21345	0.62381	-0.46827	$-0.13278 \pm i0.70677,$ $-0.11951, 0.07871$	Unstable
	1.35	0.03760	0.10497	0.44762	-0.07242	$-0.47278 \pm i1.81332$ $-0.01427 \pm i0.07318$	Stable
III	1.75	0.10911	0.17609	0.75379	0.46881	$-0.14187 \pm i0.81336,$ $-0.03768 \pm i0.10825$	Stable
IV	2.0	0.25589	0.22688	-1.42475	-1.58621	$-0.01502 \pm i0.17607,$ $-0.01494 \pm i3.77292$	Stable
	2.015	0.24531	0.20141	-1.08309	-1.22100	$0.00065 \pm i0.68099,$ $0.00080 \pm i0.08891$	Unstable
	2.0	0.06951	0.03524	-0.17544	-0.27604	$-0.00011 \pm i0.24151,$ $-0.00011 \pm i0.74499$	Stable
V	2.5	0.02513	0.00633	-0.06684	-0.12560	$-0.00092 \pm i0.61578,$ $-0.00068 \pm i1.02009$	Stable

Fig. 7 The analog circuit for the two coupled Duffing oscillators. ‘OA’s are TL082 op-amps, and ‘M’s are AD633JN multiplier ICs



stability determining eigenvalues for certain specific values of ω .

2.4 Analog simulation

The multiple resonance and anti-resonance found in the theoretical and numerical studies of the Duffing oscillator system (1) can be realized in the analog electronic circuit simulation. Figure 7 presents the analog circuit for Eq. (1) with $n = 2$. The evolution equations for the variables V_1 and V_2 obtained using the Kirchhoff’s voltage law are

$$R^2C^2 \frac{d^2V_1}{dt^2} = -\left(\frac{R^2C}{R1}\right) \frac{dV_1}{dt} - \left(\frac{R}{R2}\right) V_1 - \left(\frac{R}{100R3}\right) V_1^3 + \left(\frac{R}{RC}\right) V_2 + f \sin \omega t, \quad (13a)$$

$$R^2C^2 \frac{d^2V_2}{dt^2} = -\left(\frac{R^2C}{R1}\right) \frac{dV_2}{dt} - \left(\frac{R}{R2}\right) V_2 - \left(\frac{R}{100R3}\right) V_2^3 + \left(\frac{R}{RC}\right) V_1. \quad (13b)$$

In order to bring Eqs. (13) in dimensionless form, we introduce the change in variables $t/RC = t'$, $\omega/RC =$

ω' , $V_1 = x_1$ and $V_2 = x_2$ and then drop the primes in t' and ω' . The result is the following set of equations,

$$\ddot{x}_1 + d\dot{x}_1 + (\omega_0^2 + \delta)x_1 + \beta x_1^3 - \delta x_2 = f \sin \omega t, \tag{14a}$$

$$\ddot{x}_2 + d\dot{x}_2 + (\omega_0^2 + \delta)x_2 + \beta x_2^3 - \delta x_1 = 0, \tag{14b}$$

where $d = R/R1$, $(\omega_0^2 + \delta) = R/R2$, $\beta = R/R3$ and $\delta = R/R_C$. In Fig. 7, the values of R and C are fixed as 10 kΩ and 96.4 nF, respectively. The values of the resistors $R1$, $R2$, $R3$ and R_C can be varied to change the values of d , ω_0^2 , β and δ , respectively. We performed the analog circuit simulation of two coupled Duffing oscillators using the circuits implemented on bread board. The components in the circuit are carefully chosen with less than 1 % tolerance in the values. To obtain the response amplitudes (A_1 and A_2), fast Fourier transform (FFT) analysis on the output of each oscillator is performed using mixed signal oscilloscope Agilent MSO6014A. Small fluctuations are noted in A_i s observed in the FFT displayed in the scope. For the better accuracy, an average value of A_i s over ten measurements is obtained. The values of A_i s are displayed in dBV. It is converted into units of volt (V) using the relation $\text{dB} = 20\log\left(\frac{V}{V_0}\right)$ with $V_0 = 1.0 \text{ V}$. In the analog simulation, we fixed the circuit component values in equivalence with the values of the parameters used in the theoretical/numerical study.

Figure 8 shows response amplitudes A_1 and A_2 (in units of volts) versus ω of the two coupled Duffing oscillators circuits. The values of the parameters are as in Fig. 1. A_1 (A_2) is maximum at $\omega = \omega_r = 1.12, 1.82 \text{ krad/s}$ (1.12, 1.815 krad/s). Anti-resonance in A_1 and A_2 occurs at $\omega_{1,\text{ar}} = 1.45 \text{ krad/s}$ and $\omega_{2,\text{ar}} = 1.45 \text{ krad/s}$. These values agree very closely with

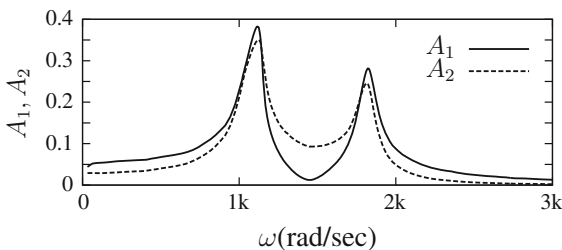


Fig. 8 Experimentally obtained response amplitude A_1 (oscillator-1) and A_2 (oscillator-2) versus the frequency ω of the input periodic signal. Here, $d = 0.1$ ($R1 = 100 \text{ k}\Omega$), $\omega_0^2 = 1$, $\beta = 1$ ($R3 = 10 \text{ k}\Omega$), $\delta = 1$ ($R2 = 5 \text{ k}\Omega$, $R_C = 10 \text{ k}\Omega$) and $f = 0.1$ (in V)

the theoretical/numerical predictions. A small deviations observed in the experimental values with theory/numeric are listed in table 2.

The effect of the coupling strength δ on the oscillator-1 and oscillator-2 of the two coupled Duffing oscillators is shown in Fig. 9a, b, respectively. In Fig. 9, we can clearly notice that the second resonance frequency, and the frequency of anti-resonance of both oscillators increase with increase in the value of δ , while the first resonant frequency of the two oscillators settles to a constant value. The results are in agreement with the theoretical prediction. It is noted that the multiple and anti-resonance are observed for small strength of non-linearity (β). For a large value of β , the corresponding controlling resistor ($R3$) in the analog circuit becomes very small. This creates the impedance mismatch in the input stage of the first integrator of the each oscillator in the coupled circuit which eventually brings down the operation of the circuit. Due to that, it is difficult to obtain hysteric frequency response curve in the analog circuit of present configuration.

3 Response of the system of n coupled oscillators

In this section, we report our investigation on system of n coupled Duffing oscillators. For the case of $n (> 2)$ coupled oscillators and by following the theoretical procedure employed for the $n = 2$ case, a set of n coupled nonlinear equations for the amplitudes A_i can be obtained. Solving them analytically or numerically is very difficult. Therefore, we analyse the case of $n > 2$ by numerically integrating Eqs. (1) and computing the amplitudes A_i s and then the response amplitudes Q_i s.

We fix the values of the parameters as $d = 0.05$, $f = 0.1$, $\omega_0^2 = 1$, $\beta = 1$ and $\delta = 1$. Figure 10 presents Q_1 versus ω for $n = 2, 3, \dots, 60$. In Fig. 10a, for the first values of n , the frequency-response curve displays clearly n distinct resonant peaks and $n - 1$ anti-resonances (minimum values of the response amplitude). The response amplitude at successive resonances in each oscillator generally decreases. For, say, $n < 10$, the last resonance peak is visible. For sufficiently large values of n , the resonance suppression and reduction in the response amplitude take place.

For the first oscillator, we numerically compute the values of the n resonant frequencies $\omega_{i,r}^{(1)}$, $i = 1, 2, \dots, n$ at which the response amplitude becomes maximum and the $n - 1$ anti-resonant frequencies $\omega_{i,\text{ar}}^{(1)}$,

Table 2 Comparison of theoretically and experimentally computed values of $\omega_{i,r}^{(j)}$ and $\omega_{ar}^{(j)}$ for the two coupled Duffing oscillators

	$\omega_{1,r}^{(1)}$	$\omega_{2,r}^{(1)}$	$\omega_{1,r}^{(2)}$	$\omega_{2,r}^{(2)}$	$\omega_{ar}^{(1)}$	$\omega_{ar}^{(2)}$
Theory	1.08	1.75	1.08	1.74	1.43	1.42
Experiment (krad/s)	1.12	1.82	1.12	1.815	1.45	1.45

Fig. 9 Experimentally obtained response amplitudes A_1 and A_2 as a function of the parameters δ and ω for the system (1) with $n = 2, d = 0.1, \omega_0^2 = 1, \beta = 1, \delta = 1$ and $f = 0.1$

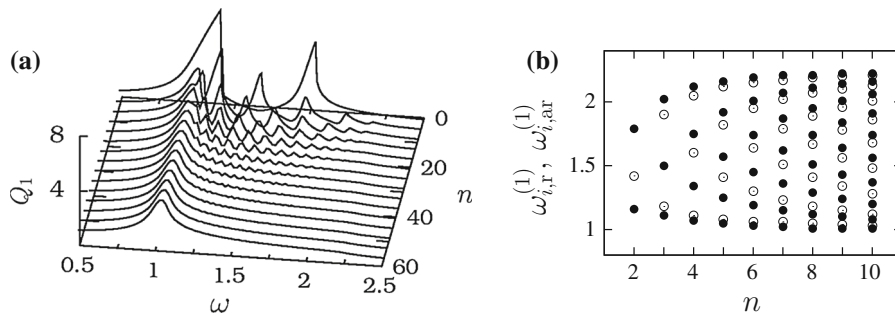
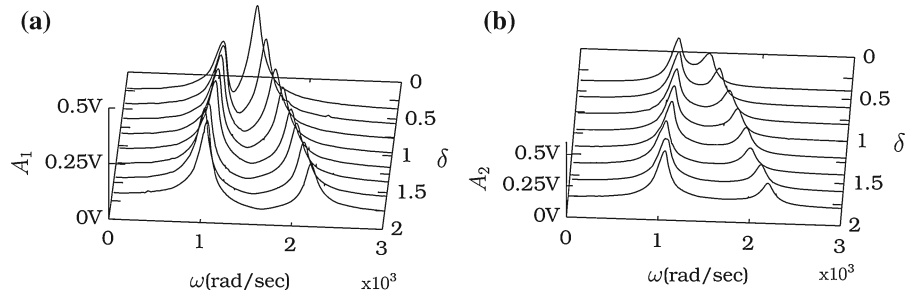


Fig. 10 **a** Frequency-response curve of the first oscillator as a function of n (number of oscillators coupled) in the system (1) for some selective values of n in the interval $[2,60]$. **b** Variation in the resonance frequencies $\omega_{i,r}^{(1)}, i = 1, 2, \dots, n$ (solid circles),

and the anti-resonant frequencies $\omega_{i,ar}^{(1)}, i = 1, 2, \dots, n - 1$ (open circles) of the first oscillator as a function of the number of oscillator n . The values of the parameters is $d = 0.05, \omega_0^2 = 1, \beta = 1, \delta = 1$ and $f = 0.1$

$i = 1, 2, \dots, n - 1$ at which the response amplitude becomes locally minimum. The result is presented in Fig. 10b for $n \in [2, 10]$. For $n = 2$ and $n = 10$, there are 2 and 10 resonances, respectively, and 1 and 9 anti-resonances, respectively. These are clearly seen in Fig 10b. A remarkable result in Fig. 10 is that as n increases from 2 the values of the first resonant frequency $\omega_{1,r}^{(1)}$, the response amplitude $Q_{1,r}^{(1)}$ at the first resonant and first anti-resonant frequency $\omega_{1,ar}^{(1)}$ decrease and approach a limiting value. For the chosen parametric values, the limiting value of $\omega_{1,r}^{(1)}$ is 1.04, which is a value close to the natural frequency $\omega_0 = 1$ of the uncoupled linear oscillators. The limiting value of $Q_{1,r}^{(1)}$ is ≈ 3.38 . The value of ω at which the last resonance takes place (denoted as $\omega_{n,r}^{(1)}$) increases with n and attains a saturation at 2.23. The response amplitude at

the last resonance decreases with n . We denote ω' and ω'' as the limiting values of the resonant frequencies of the first and the last resonance, respectively. Then, as n increases, the newer and newer resonant and anti-resonant frequencies should fall within the frequency interval $[\omega', \omega'']$ with a decreasing response amplitude at successive resonances. Essentially, the resonance profile displays an amplitude modulation. In Fig. 10a, such modulation is visible for $n \in [20, 40]$. The modulation is weak for sufficiently large values of n as is the case of $n = 60$, where the frequency-response curve shows a single resonant peak.

The response of the system of n coupled Duffing oscillators with different types of linear coupling is numerically investigated. Multiple resonances and anti-resonances are found to occur in a system of small number of coupled oscillators with a coupling of the

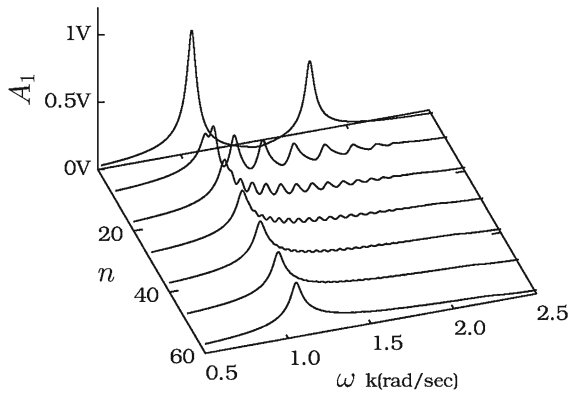


Fig. 11 Experimental frequency-response curve of the first oscillator as a function of n in the circuit corresponding to the system (1) for a few selective values of n

form $\delta(x_i - x_{i-1}) + \delta(x_i - x_{i+1})$. For the coupling of the form $\delta(\dot{x}_i - \dot{x}_{i-1}) + \delta(\dot{x}_i - \dot{x}_{i+1})$, multiple resonances and anti-resonances are not found. These resonances are observed in the case of a coupling of the form $\delta(x_{i-1} + x_{i+1})$. When all the oscillators are driven by periodic forces, then only a single resonance is obtained for the different kinds of coupling considered in the present work. It is to be remarked that the resonant behaviours observed in the system (1) are not realized in unidirectionally coupled Duffing oscillators [34].

In Sect. (2), we have presented the hardware experimental analog circuit simulation results for the two coupled Duffing oscillators. We have also performed an analog circuit simulation with $n = 60$ using Pspice circuit simulator. We preferred the circuit simulator over hardware experiments due to the difficulty in the implementation of large size circuits on circuit boards. The various features of the multiple resonance and anti-resonance observed in the numerical simulation are also realized in the analog circuit simulation. For example, the emergence of multiple resonant peaks with increase in the number of coupled oscillators observed experimentally is shown in Fig. 11. The n resonant peaks and $n - 1$ anti-resonances are clearly visible for smaller values of n .

4 Conclusion

In this paper, we have reported the occurrence of multiple resonance and anti-resonance in a system of n cou-

pled Duffing oscillators where the only the first oscillator is driven by an external periodic force with a nearest neighbour coupling. In the case of unidirectionally coupled Duffing oscillators where also the first oscillator is the only one driven by the external periodic force, the coupling is found to give rise to either an enhanced single resonance or just suppress the resonance depending upon the coupling strength [34]. One source for multi-resonance and anti-resonance is the type of coupling considered in the present work. Parametric anti-resonance [29,36], stochastic anti-resonance [24,25] and coherence anti-resonance [37] have been found to occur in certain oscillators with a single degree of freedom. Investigation of resonance and anti-resonance in n coupled versions of such oscillators with the type of coupling analysed in the present work may give rise to new and interesting results. Another kind of systems where such a study has to be performed is in excitable systems such as FitzHugh–Nagumo equations [38]. As network models may represent many physical and biological systems, it is also very important to identify the multiple resonance and anti-resonances in various network topologies.

Acknowledgments The work of R.J. is supported by the University Grants Commission, Government of India in the form of Research Fellowship in Science for Meritorious Students. The work of K.T. forms a part of a Department of Science and Technology, Government of India sponsored project Grant No. SR/S2/HEP-015/2010. M.A.F.S. acknowledges the financial support by the Spanish Ministry of Economy and Competitivity under Project Number FIS2013-40653-P.

References

1. Belbasi, S., Foulaadvand, M.E., Joe, Y.S.: Anti-resonance in a one-dimensional chain of driven coupled oscillators. *Am. J. Phys.* **82**, 32–38 (2014)
2. Wang, Y., Chik, T.W., Wand, Z.D.: Coherence resonance and noise induced synchronization in globally coupled Hodgkin–Huxley neurons. *Phys. Rev. E* **61**, 740 (2000)
3. Kenfack, A., Singh, K.P.: Stochastic resonance in coupled overdamped bistable system. *Phys. Rev. E* **82**, 046224 (2010)
4. Wu, H., Jiang, H., Hou, Z.: Array enhanced logical stochastic resonance in coupled bistable systems. *Chin. J. Chem. Phys.* **25**, 70 (2012)
5. Pikovsky, A., Zaikin, A., dela Casa, M.A.: System size resonance in coupled noisy systems and in the Ising model. *Phys. Rev. Lett.* **88**, 050601 (2002)
6. Toral, R., Mirass, C.R., Gunton, J.D.: System size coherence resonance in coupled FitzHugh–Nagumo models. *Euro-Phys. Lett.* **61**, 162 (2003)

7. Yu, H., Wany, Y., Liu, C., Deng, B., Wei, X.: Vibrational resonance in excitable neuronal systems. *Chaos* **21**, 043101 (2011)
8. Rajamani, S., Rajasekar, S., Sanjuán, M.A.F.: Ghost vibrational resonance. *Commun. Nonlinear Sci. Numer. Simul.* **19**, 4003–4012 (2014)
9. Lovera, A., Gallinet, B., Nordlander, P., Martin, O.J.F.: Mechanisms of Fano resonances in coupled plasmonic systems. *ACS Nano* **7**(5), 4527–4536 (2013)
10. Bitar, D., Kacem, N., Bouhaddi, N., Collet, M.: Collective dynamics of periodic nonlinear oscillators under simultaneous parametric and external excitations. *Nonlinear Dyn.* (2015). doi:[10.1007/s11071-015-2194-y](https://doi.org/10.1007/s11071-015-2194-y)
11. Agur, Z.: Resonance and anti-resonance in the design of chemotherapeutic protocols. *J. Theor. Med.* **1**(3), 237–245 (1998)
12. D'ambrogio, W., Fregolent, A.: The use of antiresonances for robust model updating. *J. Sound Vib.* **236**(2), 227–243 (2000)
13. Jones, K., Turcotte, J.: Finite element model updating using antiresonant frequencies. *J. Sound Vib.* **252**(4), 717–727 (2002)
14. Hanson, D., Waters, T.P., Thompson, D.J., Randall, R.B., Ford, R.A.J.: The role of anti-resonance frequencies from operational modal analysis in finite element model updating. *Mech. Syst. Signal Process.* **21**(1), 74–97 (2007)
15. Mottershead, J.E.: On the zeros of the structural frequency response functions and their sensitivities. *Mech. Syst. Signal Process.* **12**(5), 591–597 (1998)
16. Lysyansky, B., Popovych, O.V., Tass, P.A.: Desynchronizing anti-resonance effect of $m:n$ ON–OFF coordinated reset simulation. *J. Neural Eng.* **8**, 036019 (2011)
17. Uchino, K.: Piezoelectric ultrasonic motors: overview. *Smart Mater. Struct.* **7**, 273–285 (1998)
18. Jeong, W.B., Yoo, W.S., Kim, J.Y.: Sensitivity analysis of anti-resonance frequency for vibration test control of a fixture. *KSME Int. J.* **17**(11), 1732–1738 (2003)
19. Yao, G.C., Lien, N.C.: Soil–structure interaction effect on anti-resonance frequency. *J. Chin. Inst. Eng.* **24**(1), 45–54 (2001)
20. Wahl, F., Schmidt, G., Forrai, L.: On the significance of antiresonance frequencies in experimental structural analysis. *J. Sound Vib.* **219**(3), 379–394 (1999)
21. Rice, P.R., Brecha, R.J.: Cavity induced transparency. *Opt. Commun.* **126**(4–6), 230–235 (1996)
22. Sames, C., Chibani, H., Hamsen, C., Altin, P.A., Wilk, T., Rempe, G.: Antiresonance phase shift in strongly coupled cavity QED. *Phys. Rev. Lett.* **112**, 043601 (2014)
23. Blondeau, F.C.: Input–output gains for signal in noise in stochastic resonance. *Phys. Lett. A* **232**, 41–48 (1997)
24. Borkowski, L.S.: Multimodal transition and stochastic antiresonance in squid giant axons. *Phys. Rev. E* **82**, 041909 (2010)
25. Ghikas, D.P.K., Tzemos, A.: Stochastic anti-resonance in the time evolution of interacting qubits. *Int. J. Quant. Inf.* **10**(2), 1250023 (2012)
26. Audov, N.V., Krichigin, A.V.: Stochastic resonance and anti-resonance in monostable systems. *Quant. Electr.* **51**, 812 (2008)
27. Ji, L., Wei, X., Jin, Q., Yu, M.: Noise induced anticoherence resonance in a delayed circadian rhythm system. In: *Proceedings of international workshop on Chaos Fractal theories and applications*, IEEE Computer Society, p. 103 (2009)
28. Gao, Y., Wang, J.: Doubly stochastic coherence in a complex neuronal networks. *Phys. Rev. E* **86**, 051914 (2012)
29. Chakraborty, S., Sarkar, A.: Parametrically excited nonlinearity in Van der Pol oscillator: resonance, anti-resonance and switch. *Phys. D* **254**, 24–28 (2014)
30. Gluckman, B.J., Netoff, T.I., Neel, E.J., Ditto, W.L., Spano, M.L., Schiff, S.J.: Stochastic resonance in a neuronal network from mammalian brain. *Phys. Rev. Lett.* **77**(19), 4098–4101 (1996)
31. Ozer, M., Perc, M., Uzuntarla, M.: Stochastic resonance on Newman–Watts networks of Hodgkin–Huxley neurons with local periodic driving. *Phys. Lett. A* **373**, 964–968 (2009)
32. Yao, C., Zhan, M.: Signal transmission by vibrational resonance in one-way coupled bistable systems. *Phys. Rev. E* **81**, 061129 (2010)
33. Jothimurugan, R., Thamilaran, K., Rajasekar, S., Sanjuan, M.A.F.: Experimental evidence for vibrational resonance and enhanced signal transmission in Chua's circuit. *Int. J. Bifurc. Chaos* **23**(11), 1350189 (2013)
34. Rajamani, S., Rajasekar, S.: Signal amplification by unidirectional coupling of oscillators. *Phys. Scr.* **88**, 015010 (2013)
35. Press, W.H., Teukolsky, S.A., Vetterling, W.T., Flannery, B.P.: *Numerical Recipes in Fortran 77: Art of Scientific Computing*. Cambridge University Press, Cambridge (1997)
36. Tondl, A., Püst, L.: To the parametric anti-resonance application. *Eng. Mech.* **17**(2), 135–144 (2010)
37. Zhu, P., Mei, D.C.: Anti-coherence and coherence resonance induced by nonlinear time delay in autonomous stochastic system. *Eur. Phys. J. B* **87**, 109 (2014)
38. FitzHugh, R.: Impulses and physiological studies in theoretical models of nerve membrane. *Biophys. J.* **1**, 445–466 (1961)